NATIONAL AERONAUTICS AND SPACE ADMINISTRATION

Space Programs Summary No. 37-37 Volume VI

for the period November 1, 1965 to December 31, 1965

Space Exploration Programs and Space Sciences

jpl

JET PROPULSION LABORATORY
CALIFORNIA INSTITUTE OF TECHNOLOGY
PASADENA, CALIFORNIA

January 31, 1966

NATIONAL AERONAUTICS AND SPACE ADMINISTRATION

Space Programs Summary No. 37-37, Volume VI

for the period November 1, 1965 to December 31, 1965

Space Exploration Programs and Space Sciences

JET PROPULSION LABORATORY
CALIFORNIA INSTITUTE OF TECHNOLOGY
PASADENA, CALIFORNIA

January 31, 1966

Preface

The *Space Programs Summary* is a six-volume, bimonthly publication that documents the current project activities and supporting research and advanced development efforts conducted or managed by JPL for the NASA space exploration programs. The titles of all volumes of the *Space Programs Summary* are:

Vol. I. The Lunar Program (Confidential)

Vol. II. The Planetary–Interplanetary Program (Confidential)

Vol. III. The Deep Space Network (Unclassified)

Vol. IV. Supporting Research and Advanced Development (Unclassified)

Vol. V. Supporting Research and Advanced Development (Confidential)

Vol. VI. Space Exploration Programs and Space Sciences (Unclassified)

The *Space Programs Summary*, Vol. VI consists of an unclassified digest of appropriate material from Vols. I, II, and III; an original presentation of technical supporting activities, including engineering development of environmental-test facilities, and quality assurance and reliability; and a reprint of the space science instrumentation studies of Vols. I and II. This instrumentation work is conducted by the JPL Space Sciences Division and also by individuals of various colleges, universities, and other organizations. All such projects are supported by the Laboratory and are concerned with the development of instruments for use in the NASA space flight programs.

W. H. Pickering, *Director*
Jet Propulsion Laboratory

Space Programs Summary No. 37-37, Vol. VI

Prepared under Contract No. NAS 7-100, National Aeronautics & Space Administration

Contents

LUNAR PROGRAM

I. *Surveyor* Project 1

A. Introduction 1
B. Systems Testing 1
C. Flight Control 3
D. Electronics 4
E. Electrical Power Supply 4
F. Thermal Control 5
G. Engineering Mechanics 5
H. Propulsion 6
I. Ground Support Equipment 7

PLANETARY–INTERPLANETARY PROGRAM

II. *Mariner* Project 9

A. *Mariner* Mars 1964 9
B. *Mariner* Venus 1967 10
C. *Mariner IV* Command Subsystem 10

III. *Voyager* Project 11

A. Introduction 11

DEEP SPACE NETWORK

IV. Deep Space Network Systems 13

A. Introduction 13
B. Simulation Data Conversion Center 13

V. Deep Space Instrumentation Facility 14

A. Introduction 14
B. Tracking Stations Engineering and Operations 14
C. Developmental and Testing Activities 17

SUPPORTING ACTIVITIES

VI. Environmental Test Facilities 19

A. 78-Channel Constant-Bandwidth Frequency-Modulated Multiplex Magnetic Tape Recorder System 19
B. Derivation of the Mathematical Transfer Function of an Electrodynamic Vibration Exciter 21
C. Environmental Temperature Control Analysis for Radiation Cooled RF Tubes Development Test Setup 26

References 31

LUNAR PROGRAM

I. *Surveyor* Project

A. Introduction

Calculated to span the gap between the *Ranger* Project and *Apollo* Project, the *Surveyor* spacecraft is designed to take the next step in lunar technology by attempting soft landings on the Moon. The first launches will be engineering test missions to demonstrate system capability up to soft landing, and limited postlanding operations. The engineering payload includes elements of redundancy, diagnostic telemetry, touchdown instrumentation, and survey TV.

Following the engineering test missions, *Surveyor's* objectives are to extend our knowledge of lunar conditions and to verify suitability of *Apollo* landing sites.

Hughes Aircraft Company (HAC), Space Systems Division, is under contract to develop and fabricate the first seven spacecraft. The launch vehicle is a combination *Atlas/Centaur*. The JPL Space Flight Operations and Deep Space Network (Mission Operations System) will track and control the flight. The first launch is anticipated for the second quarter of 1966.

B. Systems Testing

1. SC-1 Flight Spacecraft

A special solar panel deployment test and a systems readiness test were run on SC-1 to verify that the problems experienced in the previously aborted mission sequence (*SPS 37-36*, Vol. VI, p. 1) were corrected. Two other systems readiness tests were also conducted. Vibration testing, simulating vernier engine inputs, has now been established as an additional requirement for SC-1.

An SC-1 design verification review was held to verify the adequacy of the SC-1 design. Items found to require additional action prior to launch were investigated to determine their possible effects on the success of the mission.

2. SC-2 Flight Spacecraft

Initial systems checkout of the SC-2 vehicle continued. Telecommunications, flight control, and flight control radar tests were completed prior to upgrade of the vehicle. After upgrade, the SC-2 was returned to systems

test. The retest period includes vehicle calibration, design verification, and tests required to complete initial system checkout. After completion of the retest phase, a mission-sequence electromagnetic interference test is scheduled.

3. GT-1 Group Test Vehicle

Group testing of hardware for the SP-1 (flight-quality spare subsystem set) and the SC-3 flight spacecraft continued during this period, as did retesting of upgraded hardware for the SC-1 and SC-2 vehicles. In addition, special tests were conducted to evaluate: (1) external modifications to the spacecraft receiver static-phase-error telemetry circuits, and (2) the command and data handling console photorecorder calibration.

4. T-2N-1 Descent Dynamics Test Vehicle

A successful descent test was performed using the T-2N-1 vehicle (Fig. 1). The vehicle trajectory control during free flight followed the predicted profile. During the descent, the vehicle maintained a velocity of 5 ft/sec for 4 sec. At approximately 600 ft from the ground, after a free flight from approximately 1430 ft, recovery was initiated as programmed and all recovery functions were successful. Good test data were received on all telemetry channels and optical tracking was complete. Detailed analysis of the data is being performed, after which a complete report will be issued. At the conclusion of the test, the T-2N-1 vehicle was returned to HAC for minor upgrade, inspection, and repeat of the system functional tests.

5. T-21 Prototype System Test Spacecraft

The test specification, associated procedures, and test plans have been completed for the lunar landing shock test series. The initial drop test will be conducted with an operating flight control sensor group and radar altimeter and doppler velocity sensor (RADVS) to check turnoff capability after landing shock. Dummy units are to be available for replacement if a dummy unit is destroyed during the test. A considerable effort will be made to evaluate a telemetry phase-lock problem at lunar touchdown. Preliminary tests will be conducted to evaluate performance variations due to constraints of the test location.

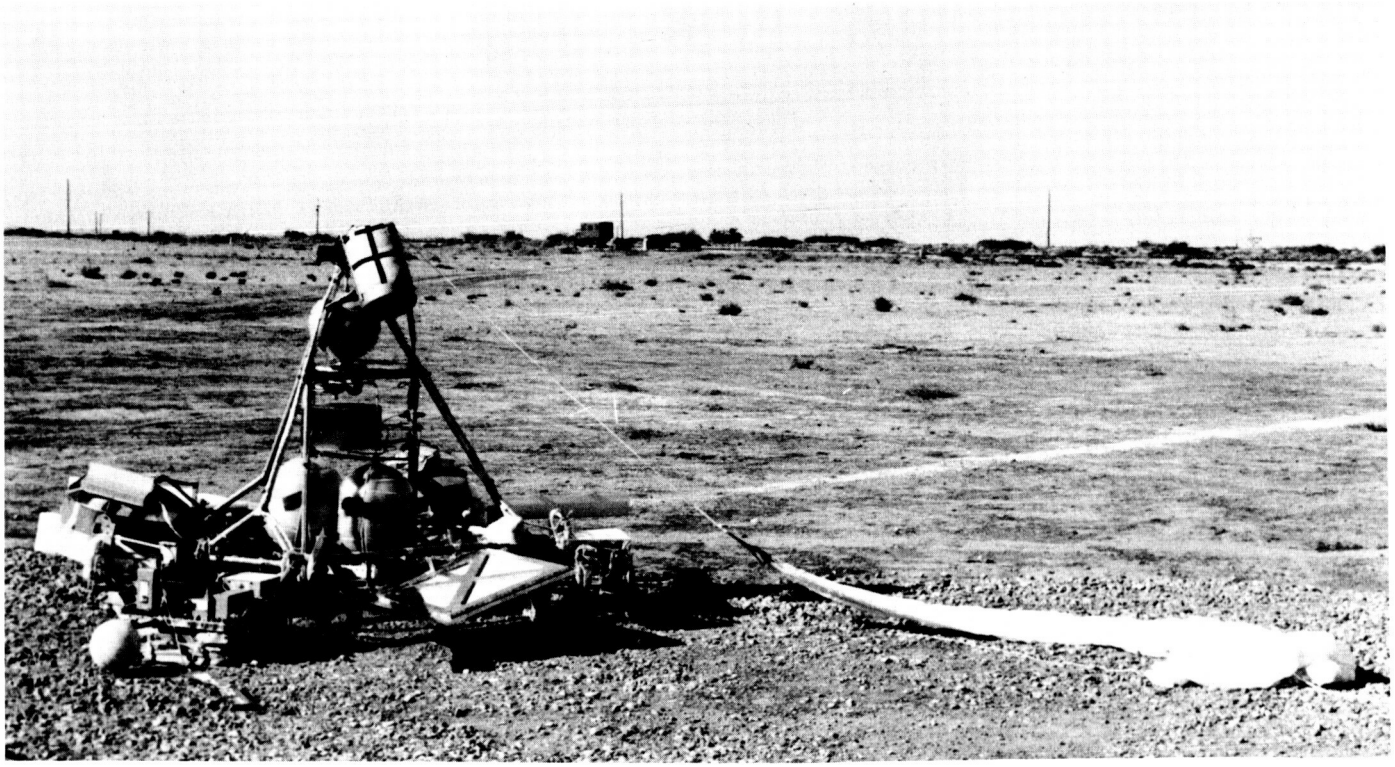

Fig. 1. T-2N-1 vehicle after successful descent test

6. S-15 Drop Test Vehicle

The S-15 drop test vehicle (Fig. 2) is being upgraded for three-dimensional landing stability tests. It has been equipped with new landing gear position potentiometers and side load strain gage assemblies. Otherwise, it is nearly identical in appearance to the T-1 dynamic stability test vehicle from which it was made.

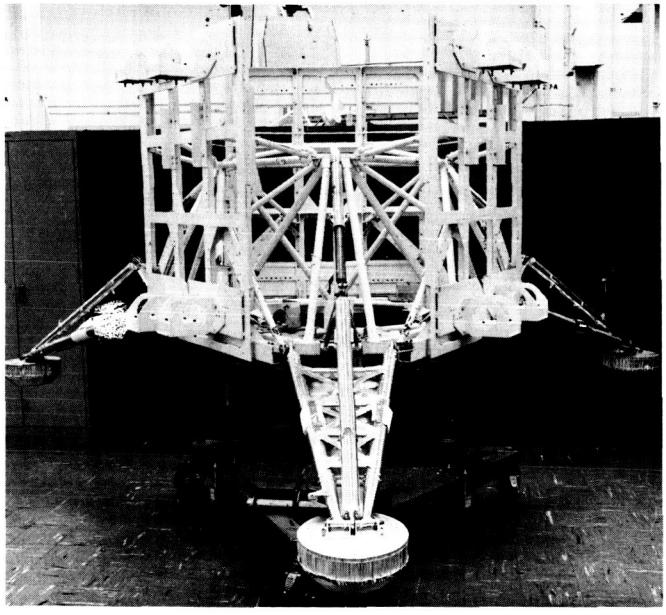

Fig. 2. S-15 drop test vehicle

C. Flight Control

1. Closed Loop Tests with S-6C Test Vehicle

Satisfactory performance of the *Surveyor* flight control system operating with a live vernier propulsion system was demonstrated during three test runs employing the S-6C flight control development test vehicle. The tests were highly successful in that they validated both the performance of the integrated systems and the method of testing.

2. Flight Control Sensor Group Testing

Flight acceptance testing was completed on the SP-1 unit, and delivery was made to the systems test area. Upgrade operations on both the SC-1 and SC-2 spacecraft resulted in both flight control sensor groups being returned to the subsystem test area. Functional performance tests for upgrade of various subassemblies were accomplished prior to disassembly.

3. T-2N Tests

T-2N flight control hardware is modified on an as-available basis to reflect the latest configuration of the SC-1 flight control hardware. Additional modifications are made to reflect unique T-2N test conditions, such as the telemetering system.

A third tether test at the Air Force Missile Development Center has demonstrated excellent performance of the inner rate loop. Transient behavior was satisfactory during engine startup and during the step from low to high thrust. Results indicated good correlation between actual and predicted system performance.

Prior to the first tether test, extensive analog computer studies were conducted and certain critical characteristics of the test were tabulated for later comparison. All possible variables of a descent test, such as release altitude, vehicle mass, measurement errors, and drag, were investigated to determine the effect of each variable on these critical characteristics.

Evaluation of flight control system performance on a "quick-look" basis could then be made by comparing the signals measured during the descent against the analog simulations of the same signals.

Quick-look results of the first tether test indicate that the flight control system controlled the T-2N-1 test vehicle within predicted limits. No vehicle or flight control system anomalies are evident.

It is concluded that the flight control system performance was satisfactory. Further evaluation with optical data will be accomplished to try to resolve the cause of the small variations in the comparisons. Further tether tests are planned for the T-2N-1 and T-2N-2 vehicles incorporating upgraded flight control hardware.

4. Flight Control Electronics Unit

During solar-thermal-vacuum testing of the SC-1 spacecraft, the retroseparation squib fired instead of another squib which was commanded to fire. It is suspected that the squib current (initiated by the command) flowing through a ground loop generated a signal suffi-

cient to fire the retroseparation squib. The circuit was subsequently modified to eliminate the ground loop and make the circuit less sensitive to voltage transients.

The flight control electronics unit, composed of the flight control programmer and flight control electronics previously on SC-1, was delivered to the subsystem test area after being modified to include circuit improvements. The flight control electronics unit previously on SC-2 is being modified to include the same circuit improvements as were incorporated in the SC-1 unit.

D. Electronics

1. Touchdown Dynamics Instrumentation Subsystem

The touchdown dynamics instrumentation subsystem provides data on spacecraft motion and loading during touchdown. All control items have been designed and are undergoing breadboard evaluation at the present time.

2. Scientific Auxiliaries

Circuit design and modification tasks were accomplished on the following four scientific auxiliaries:

(1) Micrometeorite ejecta detector auxiliary.

(2) Single-axis seismometer auxiliary.

(3) Alpha scattering auxiliary.

(4) Soil mechanics/surface sampler auxiliary.

The soil mechanics/surface sampler auxiliary breadboard unit was updated and retested over a temperature range of −40° to 110°C. All HAC-designed circuits operated within the specified limits.

E. Electrical Power Supply

1. Description

Electrical power for the *Surveyor* spacecraft is supplied by a Sun-tracking planar solar panel and a sealed, secondary silver-zinc main battery. On the first four flight spacecraft, an auxiliary battery will be utilized to provide additional peak load capability and increased energy storage capacity during transit and the lunar day. The main battery provides the electrical energy for operation during the lunar night.

The power management system is composed of a boost regulator; a battery charge regulator; and a variety of voltage converters, regulators, and power switches located in other units that provide power management for various instruments and subsystems. The battery charge regulator unit provides power conversion from the solar panel, main battery charge control, and several switching functions. The optimum-charge regulator circuit provides efficient conversion of solar panel power for use in battery charging. The battery output voltage from the unregulated bus is converted to the main regulated bus voltage by a boost regulator. A main overload trip circuit removes all nonessential spacecraft loads when an overload condition is detected. The main battery charge logic system controls the charging current to the spacecraft main battery. Normally, the system operates in the automatic mode, and the main battery is charged until its voltage reaches a predetermined level. A command mode is available for charging the battery.

The auxiliary battery control unit provides battery voltage sensing circuitry, automatic control and selection of either the auxiliary battery or both batteries, and provision for command override of the automatic control mode. A main power switch is provided for disconnecting all spacecraft power.

2. Fabrication and Test Status

Repeat flight-acceptance tests of three solar panels have been completed. Also, optimum charge regulator-solar panel integration tests were successfully conducted at the Goldstone Space Communications Stations. Cracked solar cells were found on the first three panels, but performance was degraded only slightly.

A change in main battery test methods has resulted in a significant improvement in battery pressure levels. The reliability program at the battery manufacturer has been completed. Main battery failure detected after SC-1 solar-thermal-vacuum testing is under investigation. The auxiliary battery employed in the SC-1 solar-thermal-vacuum test met performance requirements.

Modifications are being incorporated in the system test equipment assembly to allow battery parameters to be

continuously monitored during spacecraft use. These parameters include battery voltage, cell voltages, temperature, and pressure. A main battery is being prepared for the next solar-thermal-vacuum test sequence for SC-1.

Three T-2N main batteries have successfully completed flight-acceptance testing. Ten batteries incorporating the new separator system have been received from the manufacturer, and qualification of the new configuration is under way. A heater blanket has been selected for use on the T-2N recovery battery. Qualification of the recovery battery with the blanket incorporated is in progress.

Three engineering changes were incorporated into the boost regulator units for SC-1 and SC-2: (1) removal of the low voltage trip function of the overload trip circuit, (2) desensitization of the flight control *on* command to negative-going pulses, and a filter in the *Centaur/ Surveyor* separation signal input to the automatic solar panel deployment logic.

A circuit change was incorporated into the battery charge regulators to ensure reliable operation of the optimum charge regulator at high temperatures. The units performed satisfactorily up to 210°F in vacuum after the circuit change was made. Battery charge regulator units for SC-1 and SC-2 have been retrofitted and all remaining units are being upgraded.

F. Thermal Control

The *Surveyor* thermal control system provides acceptable thermal environments for all components during all phases of spacecraft operation. The passive and active methods employed include:

(1) Special preparation of spacecraft external surfaces to achieve optimum thermal absorption and emission characteristics.

(2) Provision of superinsulated compartments to house critical equipment.

(3) Provision of electrical heaters.

(4) Provision of thermal conduction paths controlled by bimetallically-operated thermal switches to maintain compartment temperatures within acceptable limits.

Four phases of SC-1 solar-thermal-vacuum testing have been completed. During these tests, the vehicle was subjected to approximately 200 hr of solar irradiation at intensity levels ranging from 77 to 112% of a nominal solar constant. Eclipses ranging from ¼ to 1¼ hr were performed during each of the phases. During one of the eclipses, the vernier propellant line heaters were commanded off 5 min before simulated vernier engine firing. The test data show that this sequence results in marginal thermal performance of the vernier lines relative to the 0°F lower limit before terminal thrusting. An engineering change request has been written to alter the mission sequence and to allow the vernier line thermal control heaters to remain on until touchdown.

A study has been initiated to compare the results of the SC-1 solar-thermal-vacuum testing with predictions made using the thermal management program. The study will provide a basis for upgrading the analytical parameters for the A-21 thermal management transit model. Following modification of the model parameters, the thermal management transit model will be considered in operational readiness for the SC-1 mission.

G. Engineering Mechanics

1. Instrumentation

Instrumentation for monitoring the vehicle angular motion just prior to and during landing has been expanded to include not only a triaxial attitude gyro system but also a triaxial rate gyro package. The additional rate information may be compared directly with data predicted by the analytical model; however, the attitude data will have to undergo Euler angle transformations to allow comparison of the three-dimensional landing test results with the computer program results. Both gyro systems are ready for use in the stability drop tests.

The load-measuring support structures for the crushable body blocks have been fabricated, and strain gages are being installed. Strain gages on the shock absorbers and rigid legs of the landing gear will measure the remaining force inputs to the vehicle. To determine vehicle longitudinal and lateral velocities at touchdown, an instrumentation package is being developed which will contain two low-frequency high-sensitivity strain gage accelerometers. The acceleration data produced by

these instruments prior to touchdown will be recorded, and during data reduction these signals will be electrically integrated to yield vehicle linear velocities. The successful comparison of test results and predicted results from the analytical model is partially dependent on the accurate determination of touchdown conditions. These accelerometer signals, along with the attitude data from the gyros, should provide the necessary information.

2. Dynamic Tests

Qualification-level variable-frequency torsion tests were performed on the S-9 structural test vehicle at JPL. Torsion pulse tests which followed the sine sweeps were completed, and the test article was returned to HAC for a posttest inspection. The test vehicle has completed manufacturing preparations for static testing. The static test setup is being prepared prior to instrumentation and calibration of the vehicle. Load application and measurements are scheduled to begin in the near future.

Preliminary tests have been conducted to determine the crushable properties of the body blocks under combined axial and lateral loading conditions. While the block was subjected to an axial crushing force, a lateral crushing force was applied through a semicircular collar at the base of the block. The tests were designed to determine the ratio of lateral force to axial force as a function of the ratio of lateral crushing velocity to axial crushing velocity. For velocity ratios in the range from 0.05 to 0.22, test results show that the lateral force is less than 7% of the axial force. Higher velocity ratios will be investigated in future tests.

H. Propulsion

1. Vernier-Propulsion-Subsystem Type-Approval Testing

All vernier-propulsion-subsystem type-approval tests on test vehicles S-6 and S-7 have been successfully completed. The performance of both vehicles was judged to be completely satisfactory. At the conclusion of type-approval testing, the S-7 vehicle was refurbished and instrumented in preparation for a pressurized drop test. The drop test was successfully completed, with all systems performing satisfactorily. Following completion of type-approval testing, some of the S-6 vehicle subassemblies were assigned for use on a flight control system verification test program.

2. Vernier-Propulsion-Subsystem Assembly Testing

Three helium tank and valve assemblies had high leakage rates after flight-assembly test vibration. The design and procedures for assembly and test were thoroughly analyzed, and corrective measures were taken. The first assembly to go through flight-assembly testing after incorporation of the corrective measures completed the postvibration high-pressure leak test with the lowest posttest leakage rate recorded on any assembly to date. No further difficulties are anticipated.

Helium tank and valve assembly type-approval testing was completed. Tests included exposure to thermal-vacuum, acceleration, and shock environments, and a proof test with leak checks after each phase.

Type-approval testing of the propellant tank assembly was begun, utilizing two new tank assemblies of flight configuration (one oxidizer and one fuel). The vibration portion and approximately one half of the thermal-vacuum phase of testing have been successfully completed.

3. Thrust Chamber Assembly (TCA) Evaluation

The evaluation of *Surveyor* vernier engines continued at the JPL Edwards Test Station. A third test to determine the suitability of the flight-type, stress-relieved wrought molybdenum nozzle material when test-fired after having been prechilled to successively lower temperatures, was performed with satisfactory results. The third test in the series (*SPS 37-36*, Vol. VI, p. 5) to demonstrate the start characteristics of an engine in a cold ultrahigh-vacuum environment was also successfully completed. The start was made in a vacuum of 4.0×10^{-4} torr with propellants conditioned to 0°F. The fourth test, with propellants conditioned to +165°F, was successfully performed in a vacuum of 4.3×10^{-4} torr.

The average ignition delay for the four tests in the series performed in a hard-vacuum environment (about 4×10^{-4} torr) was 52 msec. On the basis of TCA tests and the cold temperature tests of the S-6 type-approval system, it is concluded that the start characteristics of the TCA are acceptable if propellant temperatures (including the fuel in the jacket) are maintained in the range of 0 to 165°F.

Since lunar survival testing of the fuel thrust chamber revealed an apparent lunar storage survival limitation, additional compatibility tests of nylon (used in the valve seats) with fuel will be performed to determine the limiting conditions of temperature and exposure time to which the nylon can be subjected. The properties of other materials will also be examined to determine whether improved high-temperature exposure time could be expected with a substitute material.

Additional tests were performed to determine: (1) whether a mission profile involving continually decreasing propellant temperature would cause helium gas ingestion into the engine affecting controllability, and (2) whether propellant vapors (particularly oxidizer) in the helium pressurization lines at temperatures below −100°F would condense and freeze. The test program consisted of two simulated missions, based upon modified profiles taken from the TCA and S-6 type-approval test programs. In both mission profile tests, the pressurization lines were to be conditioned to temperatures below −100°F. The first mission profile test simulated the propellant temperature decay expected on Leg 2 of the spacecraft; the second mission profile test was conducted at a constant temperature of 100°F in simulation of the S-6 type-approval high-temperature environmental test. Both mission profiles were successfully completed, and four additional tests were then conducted. The test conditions for these were essentially the same, except that the propellants were maintained at 100°F for the full 66-hr mission.

It was concluded that there was little or no gas ingestion under constant 100°F propellant temperature conditions, and in all likelihood the anomalies noted during the high-temperature S-6 type-approval test firing were probably due to excessive bladder leakage. Additionally, it was concluded that thermal control of the cold helium pressurizing lines is acceptable and that pressurization line obstruction due to oxidizer vapor freezing will not occur.

A supplemental type-approval test program was initiated at Edwards Test Station to subject the space type-approval test engine to several nonfiring mission environments followed by several firings under simulated mission firing conditions. The first test in the series involved exposing the TCA to the nonfiring environment of static acceleration during a simulated launch. Solvent flow tests indicated no change in the throttle valve calibration or the operability of the shutoff valve.

4. *Flight Systems Support*

To ensure that the performance capabilities of the TAC's assigned to the flight program have not degraded during the various phases of pre-flight testing of the spacecraft, a set of procedures has been generated for checkout of each TCA prior to its installation on the spacecraft. To accomplish the TCA checkout, ground support equipment was designed and fabricated, including; (1) a vacuum and leak check assembly, (2) a solvent flow bench, and (3) control electronics and instrumentation. This equipment has been installed at the Eastern Test Range and is being checked out in anticipation of the receipt of SC-1.

I. Ground Support Equipment

The following design changes are being incorporated in the ground support equipment:

(1) The equipment for the scientific instrument racks in the system test equipment assembly has been redesigned.

(2) The television line selector unit in the television test rack has been redesigned to add emergency-mode capability. In addition, changes were made to increase effectiveness in the normal mode. A television light shroud, required for star mode television testing, has been designed, fabricated, and tested.

(3) The power supply used to actuate the vernier engine throttle valve for loading propellants into the vernier system tanks has been designed and built for use at the Eastern Test Range.

PLANETARY-INTERPLANETARY PROGRAM

II. *Mariner* Project

The early objective of the Planetary–Interplanetary Program was the initial probing of the planets Mars and Venus by unmanned spacecraft. The initial probing of Venus was successfully accomplished by *Mariner II*. The initial probing of Mars was successfully accomplished by *Mariner IV*. The next step in this program is a second probe of Venus by a *Mariner* spacecraft during the 1967 opportunity.

A. Mariner Mars 1964

The primary objective of the *Mariner* Mars 1964 missions was to conduct closeup (flyby) scientific observations of the planet Mars during the 1964–1965 opportunity and to transmit the results of these observations back to Earth.

A secondary objective was to provide experience and knowledge about the performance of the basic engineering equipment of an attitude-stabilized flyby spacecraft during a long-duration flight in space, farther away from the Sun than the Earth. An additional secondary objective was to perform certain field and/or particle measurements in interplanetary space and in the vicinity of Mars.

The *Mariner III* spacecraft was launched November 5, 1964. The nose cone failed to eject from over the spacecraft, thereby precluding solar panel deployment; as a result, the battery power was depleted 8 hr and 43 min after launch.

The *Mariner IV* spacecraft was successfully launched November 28, 1964, into a Mars encounter orbit. The Phase 1 portion of the *Mariner IV* flight was successfully concluded October 1, 1965, when a DC-12 command was transmitted from the Venus Station, which resulted in a transfer of the spacecraft transmitter from the high-gain antenna to the low-gain antenna. Phase 2 has been in process since that moment. The DSN is making periodic attempts, approximately once a month, to receive an RF signal from *Mariner IV* in its orbit about the Sun. The earliest significant efforts will probably take place when the new 210-ft dish antenna system at Goldstone is in operation, sometime in the spring of 1966.

On November 1, 1965, the *Mariner IV* RF signal, modulated by telemetry, was received by the Venus Station. The *Mariner IV* signal was again received December 1, 1965, and it was still modulated by telemetry. The carrier

cannot be demodulated, because the signal level is below the telemetry threshold. On December 1 the total received power was estimated to be −177.7 dbm.

If the *Mariner IV* spacecraft is operating in 1967, an attempt will be made to obtain telemetry. This effort will be carried out while simultaneously tracking the *Mariner* Venus 1967 spacecraft.

B. *Mariner* Venus 1967

The *Mariner* Venus 1967 mission was authorized in late December 1965, and the project is getting under way. Current plans call for a single launch in 1967, using a *Mariner* spacecraft (a *Mariner* Mars 1964 flight spare) modified to conform to the 1967 mission requirements, and an *Atlas/Agena* launch vehicle.

C. *Mariner IV* Command Subsystem

The performance of the spacecraft and ground command subsystems throughout the *Mariner* Mars 1964 project was quite satisfactory. All of the 85 commands transmitted to the *Mariner IV* spacecraft were executed faultlessly. The final command, transmitted October 1, 1965, established the present "command distance record" at 191 million miles.

Although the acquisition performance of the command detector was within specification limits, flight experience indicated that more rapid and more predictable command sync acquisition would be desirable. JPL has begun study of modulation/detection techniques and system implementation which incorporate rapid automatic acquisition with minimal participation required from personnel in the field.

III. *Voyager* Project

A. Introduction

1. Objectives

The primary objective of the *Voyager* Project is to carry out scientific investigations of the solar system by instrumented, unmanned spacecraft which will fly by, orbit, and/or land on the planets. Emphasis will be placed on acquisition of scientific information relevant to the origin and evolution of the solar system, the origin, evolution and nature of planetary life, and the application of this information to an understanding of terrestrial life. The primary objective of the *Voyager* missions to Mars, beginning in 1973, is to obtain information relative to the existence and nature of extraterrestrial life, the atmospheric, surface and body characteristics of Mars, and the planetary environment by performing unmanned experiments on the surface of, and in orbit about, the planet. A secondary objective is to further our knowledge of the interplanetary medium between the planets Earth and Mars by obtaining scientific and engineering measurements while the spacecraft is in transit.

2. Project Plan

All *Voyager* missions will be conducted as events of an integrated program in which each individual flight forms a part of a logical sequence in an over-all technical plan of both lander and orbital operations. The *Voyager* design will provide for the carrying of large scientific payloads to the planet, the telemetering of a high volume of data back to Earth, and long useful lifetimes in orbit about the planet and/or on the planetary surface. Hardware will be designed to accommodate a variety of spacecraft and/or capsule science payloads, mission profiles, and trajectories. Particular emphasis will be given to simple and conservative design, redundancy wherever appropriate, and a comprehensive program of component, subsystem, and system testing.

Over-all direction and evaluation of the *Voyager* Program is the responsibility of the Office of Space Science and Applications of the National Aeronautics and Space Administration. Management of the *Voyager* Project and implementation of selected systems is the responsibility of JPL, California Institute of Technology.

3. Spacecraft Description

Two *Voyager* planetary vehicles are to be designed, constructed, and tested for launch on a single *Saturn V* during the 1973 Mars opportunity. Attention is also being given to requirements imposed on such vehicles by

launches subsequent to 1973, such as a similar mission planned for 1975. Each planetary vehicle is to consist of a flight spacecraft and a flight capsule, with science experiments conducted in 1973 both from the orbiter and on the planetary surface. The flight spacecraft with its several hundred pounds of science payload will weigh approximately 2,500 lb, its retropropulsion subsystem may weigh up to 15,000 lb, and the flight capsule will weigh about 3,000 lb. The flight spacecraft will be a fully attitude-stabilized device, utilizing celestial references for the cruise phase, and will be capable of providing velocity increments for midcourse trajectory corrections and for Mars orbit attainment by both the flight spacecraft and flight capsule. Onboard sequencing and logic will be provided, as well as ground command capability. The flight spacecraft will supply its own power from solar energy or from internal sources and will be capable of maintaining radio communications with Earth. In addition, the flight spacecraft will be thermally integrated and stabilized. It will monitor various scientific phenomena near Mars and during transit and telemeter this information back to Earth; it will also monitor and telemeter data pertaining to spacecraft operation. The flight spacecraft will also provide the flight capsule with services such as power, timing and sequencing, telemetry, and command during the transit portion of the missions and may also serve as a communications relay. The sterilized flight capsule will be designed for separating from the flight spacecraft in orbit; attaining a Mars impact trajectory; entering into the Mars atmosphere; descending to the surface; surviving the impact and living on the surface 2 days in 1973 with later goals of up to 6 mo. The flight capsule will contain the power, guidance, control, communications, and data handling systems necessary to complete its mission.

No deep space-flight tests of flight spacecraft are planned. Extensive compensatory ground tests will be conducted. The test program for the flight capsule, which is planned to include Earth-entry flight tests, will investigate entry, descent, impact, communications, and sterilization.

DEEP SPACE NETWORK

IV. Deep Space Network Systems

A. Introduction

The Deep Space Network (DSN) is the NASA precision communications network designed to provide communications with, and permit control of, spacecraft designed for deep space exploration. The DSN consists of the Deep Space Instrumentation Facility (DSIF), the Space Flight Operations Facility (SFOF), and the DSN Ground Communications System (GCS).

It is the policy of the DSN to continuously conduct research and development of new components and systems and to engineer them into the DSN to maintain a state-of-the-art capability. Presently, a capability exists for simultaneous control of a newly launched spacecraft and a second one already in flight. Efforts are under way to provide for simultaneous control of either two newly launched spacecraft plus two in flight or four spacecraft in flight.

B. Simulation Data Conversion Center

The Simulation Data Conversion Center (SDCC) of the JPL Space Flight Operations Facility (SFOF) was described in *SPS 37-35*, Vol. III, pp. 31–34.

The mission-independent Phase I SDCC has been in use since mid-1965 in support of *Surveyor* and *Pioneer* Project operational tests. The Phase II Simulation Data Conversion Center development is proceeding with emphasis being placed on its timely development, including a smooth transition from the Phase I capability. The need for almost continuous use of the facility during 1966 and 1967 has modified planning so as to ensure minimum interference with operations. In particular, the Programmed Data Processor computer and other units now in use will be retained in the Phase II design. The present capability will be augmented by the addition of other units, including a larger, faster digital computer. Procurement specifications have been issued, and purchase of such a computer is anticipated in the near future.

To aid in the orderly development of the center, a new functional specification has been prepared which describes system functions on a slightly different level than that previously employed, but does not significantly alter the actual functions to be performed. Subsystems in the Phase II design are presently as follows: (1) control console, (2) data processing, (3) analog recording, (4) communications interface, and (5) mission-dependent interface. The subsystem functions described in this way serve not only to expedite the design and use of the facility in Space Flight Operations Facility internal tests, but also to facilitate its use in connection with simulation capablities to be developed at the remote sites.

V. Deep Space Instrumentation Facility

A. Introduction

The DSIF utilizes large antennas, low-noise phase-lock receiving systems, and high-power transmitters located at stations positioned around the Earth to track, command, and receive data from deep space probes. The DSIF stations are:

Station	Location
Goldstone Pioneer	Barstow, California
Goldstone Echo	Barstow, California
Goldstone Venus (research and development)	Barstow, California
Goldstone Mars (under construction)	Barstow, California
Woomera	Island Lagoon, Australia
Tidbinbilla	Canberra, Australia
Johannesburg	Johannesburg, South Africa
Madrid	Madrid, Spain
Spacecraft Monitoring	Cape Kennedy, Florida
Spacecraft Guidance and Command (under construction)	Ascension Island

JPL operates the U. S. stations, will operate the Spacecraft Guidance and Command Station, and currently plays a major role in the operation of the Madrid Station. The overseas stations are normally staffed and operated by government agencies of the respective countries with the assistance of U. S. support personnel.

The DSIF is equipped with 85-ft-diameter antennas having gains of 53 db at 2300 Mc and a system temperature of 55°K, making it possible to receive significant data rates at distances as far as the planet Mars. To improve the data rate and distance capability, a 210-ft-diameter Advanced Antenna System is under construction at the Goldstone Mars Station, and two additional antennas of this size are planned for installation at overseas stations.

B. Tracking Stations Engineering and Operations

1. Goldstone Pioneer Station

During the last week in October and the first week in November, the Pioneer Station S-band system was removed from the annex and moved into the east wing

of the control building. As with the other DSIF installation, a full basement under the control room provides for easy access to all rack interconnecting cables, and use of the cable tunnel for control, signal, and power cables to the hydro-mechanical building and the 85-ft antenna.

The permanent location of the S-band system is adjacent to the room containing the *Surveyor* ground control equipment, an arrangement that materially reduces the former long cable runs between the two equipments, and also provides for a higher order of equipment compatibility and easier coordination among personnel. Currently, system compatibility tests are being performed. Full operational and net integration testing is scheduled for early 1966.

2. Goldstone Echo Station

The *Pioneer VI* spacecraft was launched from Cape Kennedy in the early morning of December 16, 1965. Echo Station first acquired the spacecraft at 20:03:20 GMT the same day.

The first view period began with acquisition of the spacecraft at 20:03:20 GMT, December 16, 1965, and ended at 06:52:50 GMT, December 17, 1965. Eleven commands were successfully transmitted to the spacecraft from the Echo Station. A practice transfer was made with the Tidbinbilla Station, Australia, at 03:00:14 GMT, and from Tidbinbilla to the Echo Station at 04:46:50 GMT. No difficulty was experienced in either transfer procedure.

The second view period began with the spacecraft acquisition at 20:08:10 GMT, December 17, 1965, and ended at 07:04:12 GMT, December 18, 1965. The Type II orientation was performed during this period to align the spacecraft high gain antenna with the Earth. Prior to command transmissions, spacecraft control was transferred from JPL to the Echo Station at 21:20:00 GMT. A total of 198 commands was transmitted from the Echo Station to the spacecraft between 21:28:00 and 04:18:00 GMT. Spacecraft control was retransferred to JPL at 04:24:20.

After successfully completing the spacecraft orientation, the Echo Station began a daily tracking schedule.

Concurrent with preparation for, and subsequent tracking of, the *Pioneer* spacecraft, Echo Station personnel continued operational testing and interface testing of the *Lunar Orbiter* ground equipment. As the prime station at Goldstone for both *Lunar Orbiter* and the *Pioneer* space probes, the Echo Station is being readied to provide simultaneous coverage for both missions. This is being accomplished by a transfer rack assembly enabling a rapid changeover between the S-band system and either the *Lunar Orbiter* or the *Pioneer* ground equipment.

On December 14, 1965, the *Lunar Orbiter* test model spacecraft was delivered to Goldstone and installed in the spacecraft test facility shieldroom (Fig. 1). Full system operational tests to exercise the normal operation compatibility between the spacecraft electronics and the ground environment at simulated space distances will be performed.

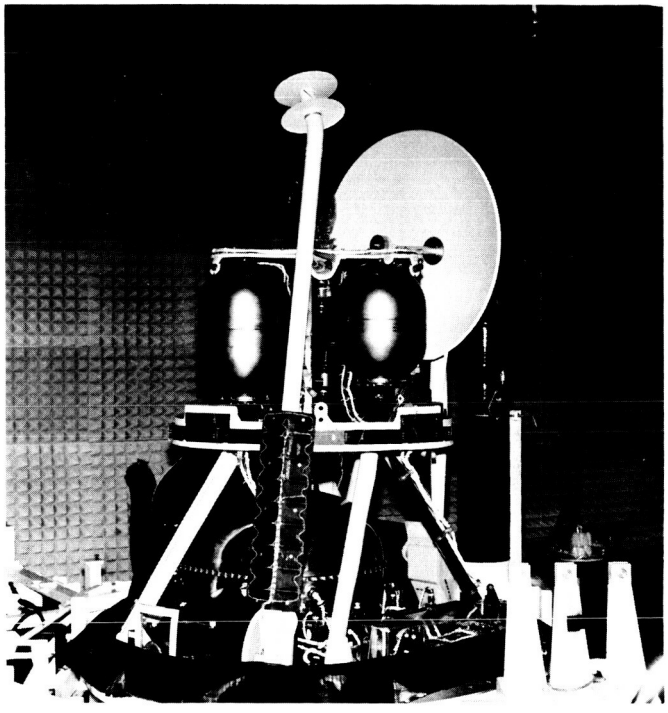

Fig. 1. *Lunar Orbiter* test model

3. Goldstone Venus Station

Two X3060 klystrons have been delivered to the Venus Station. One has been installed in a transmitter cabinet and has undergone partial acceptance testing. The transmitter cabinet houses, in addition to the klystron itself, the klystron mounting structure, cooling water plumbing and metering, filament supply, reflected power monitoring and arc detector systems and their associated RF switches, remotely driven RF drive attenuators, and various other metering and interlock circuits. By modifying

an existing transmitter cabinet, formerly used to house a smaller klystron, a considerable saving was realized, although at some sacrifice in accessibility.

Acceptance testing of the klystron at 2388 Mc (planetary radar frequency) has been completed. The results are in general agreement with those achieved in the manufacturer's acceptance tests. The remaining acceptance tests will consist primarily of investigating the tuning characteristics of the klystron. Upon completion of acceptance tests, the performance of the klystron as a dual carrier amplifier will be investigated.

The stable source described in *SPS 37-35*, Vol. III, p. 52, has been completed and tested. The stability design goal was ± 0.05 db over a reasonable temperature range and line voltage variation.

Temperature control of some of the components is necessary, as determined in tests on the individual component. The operation of the temperature control module has proved satisfactory and the fully assembled system meets the design goals set forth previously. Over-all performance indicates that the stable source will be a useful device in both the lab and field.

Testing of the experimental closed-cycle refrigerator for masers is in progress at JPL and Goldstone. Concurrently some effort is being made to simplify the instrumentation required to monitor system performance. A new technique has been derived for measuring cryogenic temperatures.

Experiments carried out with the S-band planetary radar system were open-loop ranging and total spectrum on Venus and total spectrum on Jupiter. The ranging data indicate that the actual round trip range to Venus was less than predicted, although moving into agreement with the prediction. For example, on December 13, 1965, the planet was 5.567 msec closer in round-trip range than the prediction, compared with approximately 6.6 msec 6 wk earlier.

The R&D transmitter is being reworked to accommodate the new 100-kw klystron and magnet. This amplifier is now being used for acceptance testing of the new klystron tubes.

Mariner amplifier 1 was installed in the R&D cone with an R&D VA858 klystron and has operated for a total of 820.8 filament hr and 499.5 beam hr.

The total *off* time due to failures was 12 hr, 25 min for the R&D transmitter and associated system. The major portion of this lost time was due to a failure of the high-voltage vacuum switch in the input to the high-voltage rectifier transformer; other contributors were relay failures, high-voltage cable breakdown, and reflected power coupler variations.

Operation of the Mod IV receiver has been normal with no lost time due to equipment failure. The modification to permit closed-loop operation at 2388 MHz has been completed. Further modifications of the receiver are under way to simplify operation and to improve performance.

4. Mars Station

Digital instrumentation equipment was installed in the control room on the second floor of the pedestal of the 210-ft antenna at the Mars Station. Operation and program testing is in progress. The frequency and timing subsystem was also installed and is in operation. Operations personnel are continuing servo training and maintenance training on the 210-ft antenna, conducted by Rohr Corporation personnel.

5. Woomera Station

The original reflector surface of the 85-ft tracking antenna at Woomera, Australia, was recently removed and replaced with one of better performance. The expanded aluminum mesh of the original surface had a porosity of about 70% (that is, the fraction of surface not covered by metal). The new surface consists of aluminum sheets having 25% porosity, 0.080-in. thick, for the inner two-thirds of the area, and 50% porosity, 0.080-in. thick, for the two outer "rings." System performance is improved first by a decrease in system temperature of about 4°K, and then by an increase in gain of approximately 0.6 db. The total system temperature is now about 44°K, and aperture efficiency is 0.65.

6. Tidbinbilla Station

An aircraft masking exercise was conducted at Tidbinbilla Station to determine the effect on spacecraft communications caused by aircraft flying through the line-of-sight beam between the Station tracking antenna and the spacecraft. It was concluded that the DC3 aircraft passing through the beam, with the associated masking of the received *Mariner IV* signal, did not significantly affect reception of full tracking and telemetry data from the spacecraft.

7. Spacecraft Guidance and Command Tracking Station

Following the initial integration of the Spacecraft Guidance and Command system components at Goldstone, the equipment was dismantled and packed for overseas shipment. The equipment was transported to Ascension Island in mid-October via two chartered cargo aircraft. Acquisition aid equipment for the 30-ft antenna has been installed and partially tested; equipment necessary for boresight and final RF measurements is not yet available at the site. Final tests will be made after the station is completed, as all subsystems must be operational before final boresighting, snap-on, and tracking tests are performed.

C. Developmental and Testing Activities

1. Multiplier Chains (Phase and Amplitude Stability)

Typical multiplier and very high frequency amplifier units comprising a complete S-band chain have been evaluated individually and in combination, with respect to phase and amplitude stability versus ambient temperature and RF drive level. In all cases, phase shift measurements were conducted at the output S-band frequency, and the phase stability referred to the output of the test chain was recorded. Measurements indicate that all units can be expected to perform satisfactorily under service conditions and that the maximum phase shift of a complete S-band $\times 75$ multiplier chain over a 10-hr tracking period can be expected to amount to approximately 800 deg. The evaluation of these multiplier chains, currently in use at the S-band radar site, also establishes typical performance estimates of the X-band system (excepting the final $\times 4$), inasmuch as the design is essentially identical.

2. Microwave Maser Development

The development of techniques which improve the performance of masers has resulted in a traveling wave maser (TWM) structure which can be fabricated from a solid piece of copper. The TWM structure has no joints which might result in loss of microwave signal power, or which might restrict the transfer of heat from the maser material to the cooled flange of the TWM.

A one-piece comb-type maser structure is shown in Fig. 2. The cover (with tuning screws), a typical ruby slab, an isolator strip, and a temperature sensor are also shown. The sensor is a carbon resistor, held between two copper discs which mount on the TWM. Tests indicate that there is adequate heat transfer through the solid copper structure.

Fabrication of the TWM involved conventional machining techniques. Difficulty was encountered in holding uniform dimensions in the comb area, so tuning screws for the resonant fingers were used to compensate for the lack of machining precision. Successful machining techniques were subsequently developed by the JPL machine shop, resulting in a practical and accurate process for TWM fabrication. The use of a shaper, a machine that removes metal with a scraping process, has produced an excellent surface finish and uniformity of 0.0001 in. in the most critical area of the comb structure.

More recently, the use of electric discharge machining for metal removal between the fingers of the comb has enabled the fabrication of structures with close interval and long finger length.

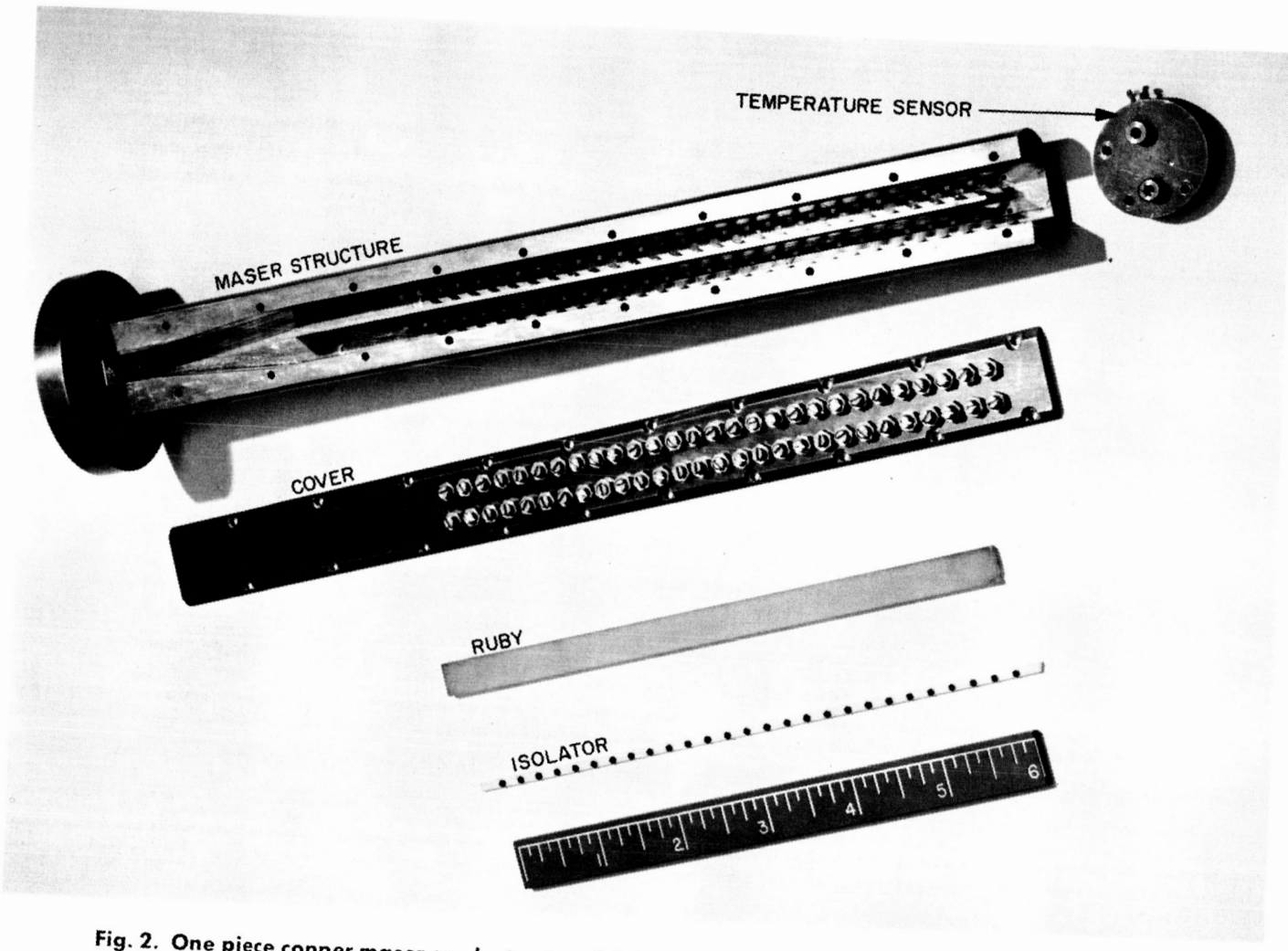

Fig. 2. One piece copper maser comb structure fabricated with conventional machining techniques

SUPPORTING ACTIVITIES

VI. Environmental Test Facilities

A. 78-Channel Constant-Bandwidth Frequency-Modulated Multiplex Magnetic Tape Recorder System

1. Introduction

Due to the increased number of data channels needed for general spacecraft vibration testing at the JPL Environmental Test Laboratory, a high-channel-capacity magnetic tape recorder system (Fig. 1) was implemented in order to supplement the present recording capability. In comparison with the existing 14-channel conventional frequency-modulated (FM) tape recorder systems, this system offers the following advantages:

(1) Six times more channels per tape transport, resulting in operational simplicity, as well as smaller system space per channel.

(2) Lower cost in initial implementation, as well as in operation (magnetic tape cost).

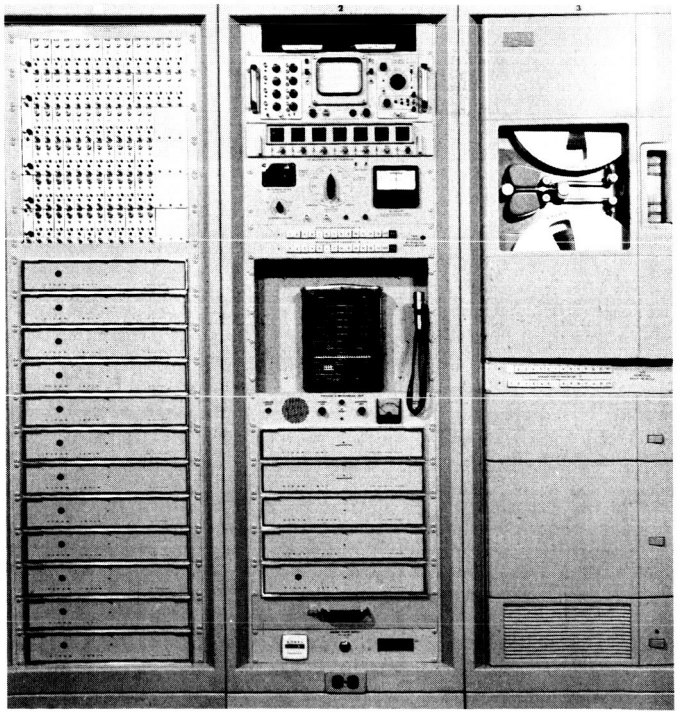

Fig. 1. 78-channel magnetic tape recorder system

(3) Faster system setup and checkout operations due to the use of a special system calibrator, preprogrammed patch board, and various multiposition switches. The overall checkout time averages about 8 min (6 sec per channel).

(4) Greater accuracy due to the use of stable solid-state circuitry. For instance, amplitude drift was within ±0.2% of full scale for all channels over a 4-month period of daily operation without an adjustment.

(5) Better control of interchannel phase error due to the use of the FM multiplex method. For each 6-channel group (i.e., one tape track), the relative phase error is within 10-μsec peak-to-peak (i.e., 7.2 deg peak-to-peak at 2 kHz).

(6) A DC −2kHz flat response on all 78 channels with high degree of conformity.

2. Description

The system basically consists of four groups of equipment: (1) voltage-controlled oscillator (VCO)-multiplexer (record), (2) tape recorder/reproducer, (3) demultiplexer-discriminator (playback), and (4) other operational hardware (for calibration, patching, voice annotation, monitoring, and cabling). Each tape track is associated with an identical six-channel record and playback system, making up 78 identical record channels (13 tape tracks) and 12 playback channels (2 tape tracks). The two playback systems can be switched into any of the 13 tape tracks for calibration, monitoring, or playback. The 14th tape track (300 Hz to 300 kHz) can be used for reference frequencies, timing, and control, and the 15th track can be used for voice. A single-record and playback block diagram is shown in Fig. 2.

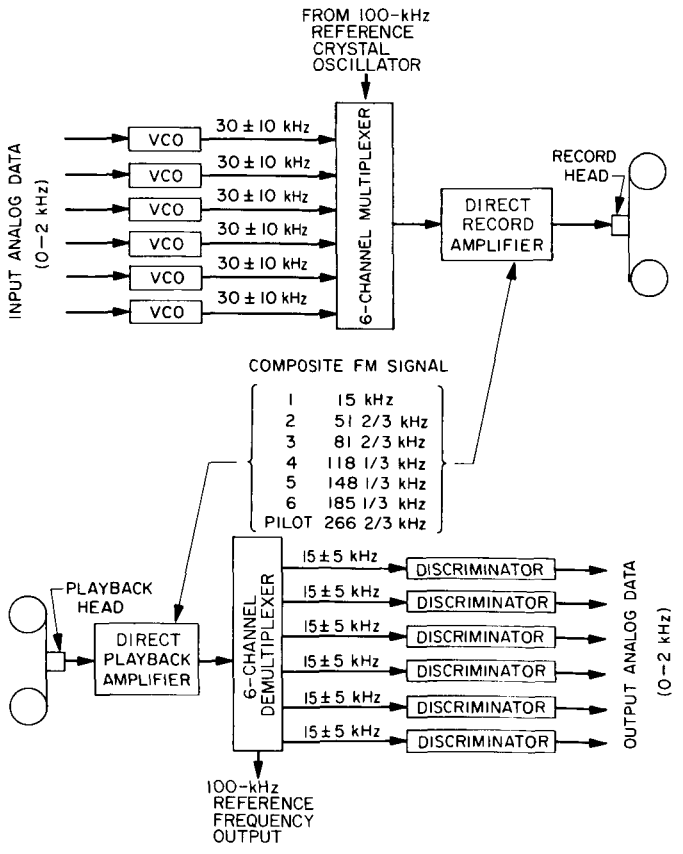

Fig. 2. Single-record and playback block diagram

a. Record. Six identical VCOs convert analog input voltages to proportional frequency pulse trains. The VCOs operate at a center frequency of 30 kHz with peak deviations of ±10 kHz (±33⅓%). The output pulse trains and a 100-kHz reference frequency are fed to a multiplex unit. The multiplex unit performs waveshaping of the VCO outputs and, with translation frequencies derived from the 100-kHz reference frequency, heterodyne each VCO output to a particular frequency band between 9 and 200 kHz. The pilot carrier (266⅔ kHz) is also derived from the 100-kHz reference frequency and mixes into the composite output.

b. Playback. The output from a single track of the tape recorder is passed through a demultiplex unit, whose operation is just the reverse of that of the multiplex unit. The pilot carrier is separated from the composite signal and is used to generate translation frequencies to heterodyne the various carriers back to their original positions in the frequency spectrum. The played-back 100-kHz reference is available at that point. The six separate channels are then applied to six identical FM discriminators (15 ± 5 kHz).

c. Setup/checkout. The system calibrator, used in the setup operation, has precision voltage, frequency sources, and a null detector meter with a resolution of the order of 0.1% of full-scale data. First, 12 discriminators are checked for zero and ±full scale by the calibrator, and then the 78 VCOs are checked utilizing the 12 discriminators in conjunction with the calibrator for zero and ±full scale. A rapid multichannel checkout is accomplished in two steps by sequential switching of the channels to the null detector and two preprogrammed patch boards. For the initial setup, there are only three adjustments per channel: VCO zero; VCO gain adjustment, where the input has a range of ±0.5 to ±5-v peak per full scale; and discriminator zero adjustment. The discriminator output is fixed to ±1.414-v peak per full scale.

d. Operation. The system is operational after the rapid checkout and the insertion of an operational program board. During data acquisition, the incoming and reproduced data can be monitored, six channels at a time, by the monitoring oscilloscopes. A spot check of 78 channels averages approximately 12 sec. During operation, any switches in front, other than the master power and tape transport switches, can be manipulated in any manner without influencing the recording.

B. Derivation of the Mathematical Transfer Function of an Electrodynamic Vibration Exciter

1. Abstract

The transfer function of an electrodynamic vibration system (power amplifier and vibration exciter) is defined as the ratio of table accelerations to input voltage. The equation is itself a function of frequency. An input signal with a given frequency is applied to the input of the system; the signal appears at the output, multiplied by the magnitude of the transfer function, with its phase shifted by the phase angle of the transfer function.

This article presents a detailed solution of the mathematical equation that describes a typical electrodynamic vibration system. The mathematical analysis is compared with the empirical transfer function of a particular vibration exciter to demonstrate the validity of the equation and the value of mathematics and computers for analysis of vibration techniques.

2. Introduction

Transfer functions of a vibration system can be obtained empirically by plotting the voltage required by the system to maintain a certain (constant) acceleration level. It is a more difficult task to obtain the transfer function by mathematical methods. A mathematical transfer function of a vibration system is a desirable equation and valuable tool for investigating the dynamics of these systems, and in particular, the equation is important in the analysis, synthesis, or modification of control techniques for single or multiple shaker systems.

Although mathematical transfer functions of vibration systems have appeared in the literature from time to time, there have been two problems associated with these equations:

(1) There have been errors in the equations in some cases.

(2) The derivations have not been included, or if included, are either not obvious or not complete.

3. The Analog Circuit

The equivalent electrical circuit for an electrodynamic shaker (Fig. 3) is used quite often for analysis and synthesis of vibration systems[1] (Ref. 1). In this figure,

v_d = driver coil voltage, volts

i_d = driver coil current, amperes

R_d = driver coil resistance, ohms

L_d = driver coil inductance, henrys

K_g = force constant, newtons/amperes
(The ideal transformer with turns ratio K_g:1 provides the electromechanical conversion.)

M_c = mass of the driver coil, kilograms

M_t = table mass, kilograms

$1/K_t$ = table compliance, meters/newton

$1/K_f$ = flexure compliance, meters/newton

[1]Ling Electronics Division, Anaheim, California, and MB Electronics Company, New Haven, Connecticut—two prominent manufacturers of vibration equipment—have used this equivalent circuit in their literature.

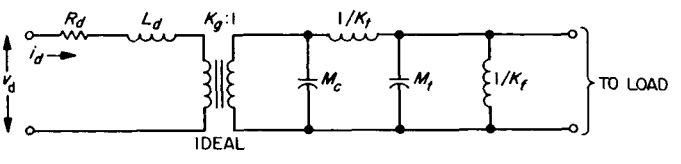

Fig. 3. Equivalent electrical analog circuit for an electrodynamic shaker

The following relationships will transform the above mechanical terms into analog electrical terms:[2]

$1/K \rightarrow$ L: inductance, henrys

$M \rightarrow$ C: capacitance, farads

$F \rightarrow$ I: current, amperes

$\dot{x} \rightarrow$ V: voltage, volts

$\ddot{x} \rightarrow \frac{d}{dt}V = SV$: time derivative of voltage

The subscripts from the mechanical system are carried over to the electrical analog. Also, $S = d/dt$ and $1/S = \int dt$, where S is the Laplace transform variable.

Since the equivalent electrical circuit has an ideal transformer with turns ratio K_g:1, it is necessary to refer the secondary side of the transformer over to the primary side. This can be done in the following manner (Ref. 3):

(1) Multiply inductances by K_g^2.

(2) Multiply capacitances by $1/K_g^2$.

The resulting equivalent electrical circuit is shown in Fig. 4.

The voltage at node ② is $V_{2L_f} = SK_g^2 L_f I_3$.

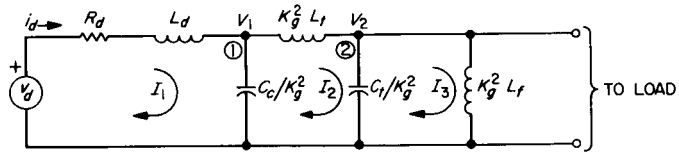

Fig. 4. Reflected equivalent electrical analog circuit

The voltage transfer function of the circuit (Fig. 2) is V_{2L_f}/v_d. To obtain this transfer function, it is necessary to calculate I_3.

For the analog system, voltage is equal to velocity. The velocity at node ② is $\dot{x}$. The acceleration at node ② is $\ddot{x}$, where x is the displacement. Therefore, $dx/dt = Sx$ is the velocity and $d^2x/dt^2 = S^2x$ is the acceleration. Again, the velocity at node ② (the voltage of the analog system) is $SK_g^2 L_f I_3$. The acceleration at node ② is $S^2K_g^2 L_f I_3$. The voltage transfer function, in terms of acceleration, is defined as

$$\frac{\ddot{x}_2}{v_d} \text{ or } \frac{S\dot{x}_2}{v_d} \text{ or } \frac{SV_2}{v_d}$$

4. Modification of the Analog Circuit

Physically, however, there is not too much interest in the acceleration of the flexures; but, there is interest rather, in the acceleration of the vibration table. Although the acceleration at node ② is the same as that for the flexures, the forces (currents in the analog system) are different

$$V_{2C_t} = \frac{1}{S(C_t/K_g^2)}(I_2 - I_3)$$

For the physical interpretation of the analog circuit, it may be better to redraw the circuit as shown in Fig. 5.

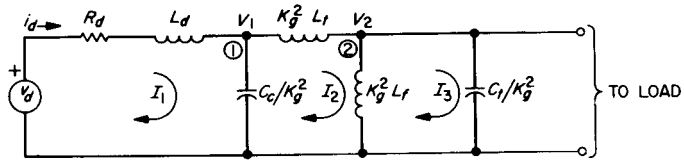

Fig. 5. Modified equivalent electrical analog circuit

5. Derivation of the Transfer Function

In the new circuit, the velocity of the vibration table is

$$V_{2C_t} = \frac{1}{S(C_t/K_g^2)} I_3$$

To obtain the acceleration of the table, it is only necessary to multiply the above equation by the Laplace operator S

$$S\,V_{2C_t} = \frac{S}{S(C_t/K_g^2)} I_3 = \frac{K_g^2 I_3}{C_t}$$

The table acceleration is

$$\ddot{x}_2 = \frac{K_g^2 I_3}{C_t} \qquad (1)$$

where I_3 is as defined in Fig. 5. The ratio $\ddot{x}/v_d$ is needed to obtain the mathematical transfer function.

[2]The force-current analogy system is employed because, from the point of view of physical interpretation, it is the only natural analogy (Ref. 2).

By writing Kirchhoff's voltage equations (loop equations), a matrix $[z]$ can be constructed

$$\begin{bmatrix} (R_d + SL_d + K_g^2/SC_c) & -K_g^2/SC_c & 0 \\ -\frac{K_g^2}{SC_c} & \left(\frac{K_g^2}{SC_c} + SK_g^2L_t + SK_g^2L_f\right) & -SK_g^2L_f \\ 0 & -SK_g^2L_f & \left(SK_g^2L_f + \frac{K_g^2}{SC_t}\right) \end{bmatrix} \cdot \begin{bmatrix} I_1 \\ I_2 \\ I_3 \end{bmatrix} = \begin{bmatrix} v_d \\ 0 \\ 0 \end{bmatrix}$$

$$I_3 = \frac{\begin{vmatrix} \left(R_d + SL_d + \frac{K_g^2}{SC_c}\right) & -\frac{K_g^2}{SC_c} & v_d \\ -\frac{K_g^2}{SC_c} & \left(\frac{K_g^2}{SC_c} + SK_g^2L_t + SK_g^2L_f\right) & 0 \\ 0 & -SK_g^2L_f & 0 \end{vmatrix}}{\Delta_z}$$

where Δ_z is the determinant of the $[z]$ matrix.

The numerator of I_3 can be solved by expanding around v_d, since the third column has 2 zeros

$$I_{3\ numerator} = v_d\left(\frac{K_g^2}{SC_c} \cdot \frac{SK_g^2L_f}{1}\right)$$

$$= v_d\,(K_g^4L_f/C_c)$$

Therefore

$$I_3 = \frac{(K_g^4L_f/C_c)\,v_d}{\Delta_z} \qquad (2)$$

By substituting Eq. (2) into Eq. (1), the table acceleration becomes

$$\ddot{x}_2 = \frac{v_d\,(K_g^4L_f)/C_c}{\Delta_z}\left(\frac{K_g^2}{C_t}\right)$$

By dividing both sides of the above equation by v_d, the ratio $\ddot{x}_2/v_d$ is obtained, which is the transfer function of an electrodynamic vibration system

$$\frac{\ddot{x}_2}{v_d} = \frac{K_g^6L_f/C_cC_t}{\Delta_z} \qquad (3)$$

Consider Δ_z

$$\Delta_z = \begin{vmatrix} (R_d + SL_d + K_g^2/SC_c) & -K_g^2/SC_c & 0 \\ -K_g^2/SC_c & \left(\frac{K_g^2}{SC_c} + SK_g^2L_t + SK_g^2L_f\right) & -SK_g^2L_f \\ 0 & -SK_g^2L_f & (SK_g^2L_f + K_g^2/SC_t) \end{vmatrix}$$

Expanding Δ_z around the third row

$$\Delta_z = SK_g^2L_f \begin{vmatrix} R_d + SL_d + K_g^2/SC_c & 0 \\ -K_g^2/SC_c & -SK_gL_f \end{vmatrix} + (SK_g^2L_f + K_g^2/SC_t)$$

$$\cdot \begin{vmatrix} (R_d + SL_d + K_g^2/SC_c) & -K_g^2/SC_c \\ -K_g^2/SC_c & \left(\frac{K_g^2}{SC_c} + SK_g^2L_t + SK_g^2L_f\right) \end{vmatrix}$$

Expanding Δ_z

$$\Delta_z = \frac{K_g^4L_fR_d}{C_c} + S^2K_g^4L_fR_dL_t + \frac{SK_g^4L_fL_d}{C_c} + S^3K_g^4L_fL_dL_t + \frac{SK_g^6L_fL_t}{C_c}$$

$$+ \frac{R_dK_g^4}{S^2C_cC_t} + \frac{R_dK_g^4L_t}{C_t} + \frac{R_dK_g^4L_f}{C_t} + \frac{L_dK_g^4}{SC_cC_t} + \frac{SK_g^4L_dL_t}{C_t} + \frac{SK_g^4L_dL_f}{C_t}$$

$$+ \frac{K_g^6L_t}{SC_cC_t} + \frac{K_g^6L_f}{SC_cC_t}$$

The next step is to put Δ_z over a common denominator and collect terms with reference to the power of S. By inspection

$$\Delta_{z\ denominator} = S^2C_cC_t$$

$$\Delta_{z\ numerator} = S^5 + S^4\left(\frac{R_d}{L_d}\right) + S^3\left(\frac{1}{L_tC_c} + \frac{K_g^2}{L_dC_c} + \frac{1}{L_fC_t} + \frac{1}{L_tC_t}\right)$$

$$+ S^2\frac{R_d}{L_d}\left(\frac{1}{L_tC_c} + \frac{1}{L_fC_t} + \frac{1}{L_tC_t}\right)$$

$$+ S\frac{1}{C_cC_t}\left(\frac{1}{L_fL_t} + \frac{K_g^2}{L_dL_f} + \frac{K_g^2}{L_dL_t}\right) + \frac{R_d}{L_fL_dL_tC_cC_t}$$

Dividing $\Delta_{z\ denominator}$ by $K_g^4L_fL_dL_tC_cC_t$, it becomes

$$\Delta_{z\ denominator} = \frac{S^2}{K_g^4L_fL_dL_t}$$

The acceleration of the table is

$$\ddot{x}_z = \frac{K_g^2I_3}{C_t} \tag{4}$$

The force of the table is

$$I_3 = \frac{(K_g^4L_f/C_c)\,v_d}{\Delta_z} \tag{5}$$

The desired transfer function is

$$\frac{\ddot{x}_z}{v_d} = \frac{K_g^6L_f/C_cC_t}{\Delta_z} \tag{6}$$

if Δ_z is defined

$$\Delta_z \equiv \frac{P}{S^2/K_g^4L_fL_dL_t}$$

where P is the fifth-order polynomial ($\Delta_{z\ numerator}$). Then substituting Δ_z into Eq. (6) gives

$$\frac{\ddot{x}}{v_d} = \frac{K_g^6L_f}{C_tC_c} \cdot \frac{1}{P/(S^2/K_g^4L_fL_dL_t)}$$

or

$$\frac{\ddot{x}_2}{v_d} = \frac{K_g^6 L_f}{C_t C_c} \cdot \frac{S^2}{P\,(K_g^4 L_f L_d L_t)}$$

this becomes

$$\frac{\ddot{x}_2}{v_d} = \frac{S^2 K_g^2}{(C_t C_c L_d L_t) P}$$

so that

$$\frac{\ddot{x}_2}{v_d} = \frac{S^2 K_g^2 / C_t C_c L_d L_t}{P}$$

where, again, P is the fifth-order polynomial which is the numerator of Δ_z, and $\ddot{x}_2/v_d$ is the mathematical voltage transfer function of the electrodynamic shaker system that has an equivalent electrical analog circuit such as that of Fig. 3.

For the mechanical engineer who prefers mechanical terms rather than electrical terms to describe a transfer function, the function can be transformed back to what it was using the analogy in reverse, obtaining

Table 1. Shaker constants of MB Electronics Company C-10E exciter

Constant	Value	Meter kilogram second units
K_t	8.16×10^5	newtons/meter
K_f	6.30×10^5	newtons/meter
M_c	1.815	kilograms
M_t	6.120	kilograms
L_d	1.2×10^{-3}	henrys
R_d	3.0	ohms
K_g	190.0	newtons/ampere

The results suggest, among other things, that perhaps the digital computer could be utilized to design or modify electrodynamic vibration exciters. It should be a very simple procedure to optimize a transfer function by computer techniques. The computer program can be quite simple (Ref. 6), and the computer time to do this should not run over 4 min at the very most. All this presupposes an accurate mathematical model. Nothing

$$\ddot{x}/v_d = \frac{S^2 K_g^2 K_t / M_c M_t L_d}{S^5 + S^4\left(\frac{R_d}{L_d}\right) + S^3\left(\frac{K_t}{M_c} + \frac{K_g^2}{L_d M_c} + \frac{K_f}{M_t} + \frac{K_t}{M_t}\right) + S^2 \frac{R_d}{L_d}\left(\frac{K_t}{M_c} + \frac{K_f}{M_t} + \frac{K_t}{M_t}\right)}$$

$$+ S\,\frac{1}{M_c M_t}\left(K_f K_t + \frac{K_g^2 K_f}{L_d} + \frac{K_g^2 K_t}{L_d}\right) + \frac{R_d K_f K_t}{M_c M_t L_d}$$

6. Comparison with Empirical Data

Transfer functions are frequently expressed in terms of the Laplace transform variable S (Ref. 4), as above. For steady state sinusoidal conditions, the Laplace variable S can be replaced by the operator $j\omega$, where $\omega = 2\pi F$ and $j = \sqrt{-1}$.

A computer program was written (Ref. 5) and an IBM 7090 was utilized to test the mathematical model of the vibration system, using the shaker constants of an MB Electronics Company C-10E exciter. Table 1 lists the constants specified by the manufacturer.

Fig. 6 illustrates the results obtained by comparing the acceleration-vs-voltage plot obtained from the MB Electronics Company C-10E exciter (bare table) with that predicted by the computer with the analytically derived transfer function.

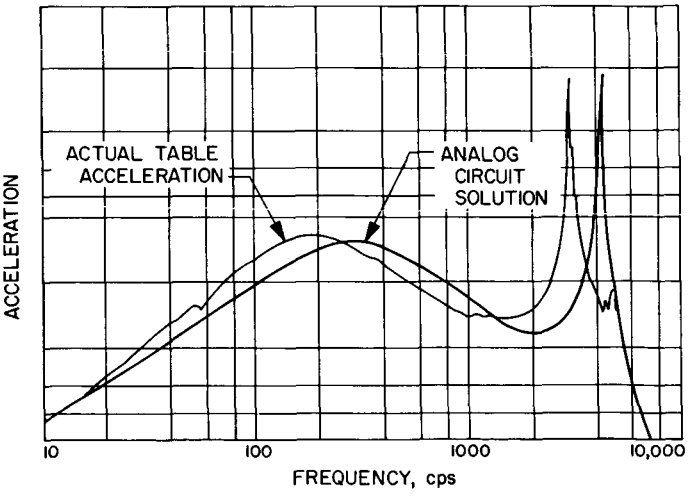

Fig. 6. Empirical transfer function vs mathematical transfer function of an electrodynamic vibration system

is gained by having three models: one for the low frequencies, one for the midrange, and another for the high frequencies. In fact, the mathematical transfer function will suffice for all frequencies.

7. Conclusions

The close correlation between the mathematical transfer function and the empirical transfer function suggests the validity of the mathematics and the analog circuit and the value of using mathematical and computer techniques to analyze and synthesize vibration systems. It is important, however, that the model and mathematical equations be exact in order to produce meaningful results.

By extending the analog circuit and utilizing the techniques described in this article, it should be possible to investigate the dynamics of a multiple shaker system with an attached resonant load. Such a study has been initiated and the results are encouraging.

Other studies should be performed to indicate solutions to control problems associated with electrodynamic exciters being employed for shock testing and multiple shaker configurations.

C. Environmental Temperature Control Analysis for Radiation Cooled RF Tubes Development Test Setup

A new design radiation cooled RF traveling wave tube for spacecraft application is being developed by the Spacecraft Radio Section of JPL. Prototype models of the tube are being fabricated.

A series of tests will be performed on the prototypes, at the Environmental and Dynamic Testing Laboratory, to study their thermal characteristics. The test program will entail operation of the tubes while in high vacuum at various temperature environments.

In preparation for the testing, a preliminary analytical study has been completed by the environmental laboratory to determine:

(1) The effect of various temperature environments on the tube heat transfer characteristics.

(2) If the test program can be conducted in standard 30 × 50-in. vacuum chambers without extensive modifications.

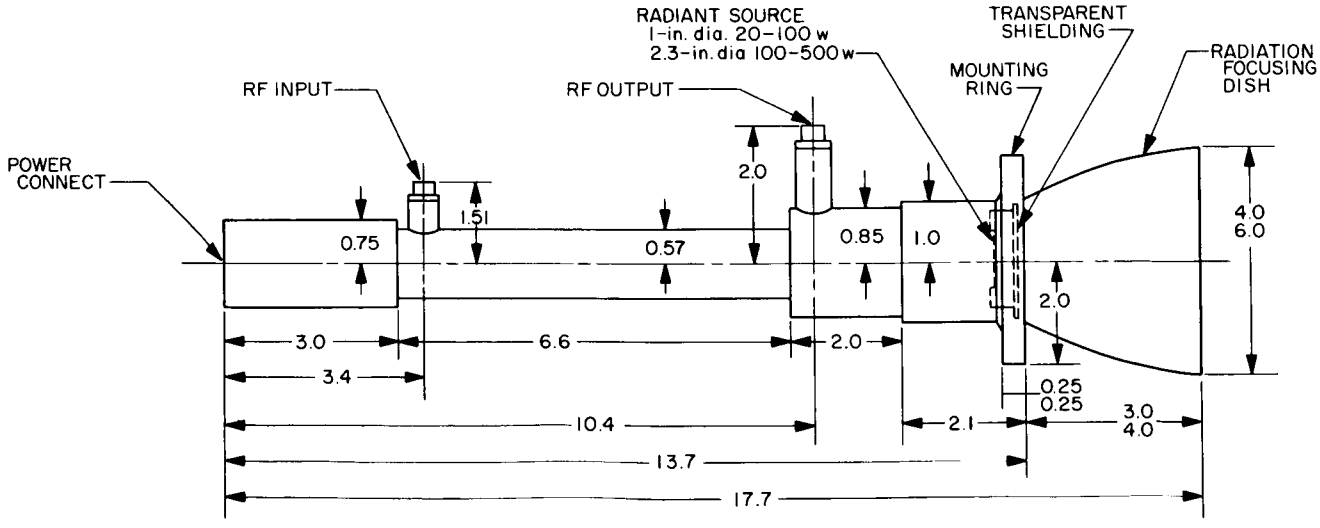

NOTES:
1. DIMENSIONS IN in., UPPER, 20-100 w; LOWER, 100-500 w.
2. RF CONNECTIONS: INPUT: STRAIGHT OUT N TYPE; CABLE SIZE RG 55; MINIMUM BENDING RADIUS 3 in. OUTPUT: STRAIGHT OUT TNC TYPE; CABLE SIZE RG 9; MINIMUM BENDING RADIUS 6 in.
3. DC POWER: 3000 v 20-100 w; 4000 v 100-500 w.
4. TUBE 50% EFFICIENT; 90% OF HEAT PRODUCED RADIATED BY RADIANT SOURCE AND 10% CONDUCTED BY MOUNTINGS AND RADIATED BY REST OF TUBE.

Fig. 7. Traveling wave tube design

Table 2. Surface characteristics

Surface	Emissivity			Absorptivity			Reflectivity		
	ϵ_1	ϵ_2	ϵ_3	α_1	α_2	α_3	ρ_1	ρ_2	ρ_3
Tube 20–100 w[a]	0.9			0.9			0.1		
Tube 100–500 w[a]	0.9			0.9			0.1		
Chamber walls			0.2			0.2			0.8
Cold plate		0.9			0.9			0.1	

[a]These figures might not correspond with the final specifications for the tubes since the tubes are being developed.

The analysis consisted of two parts. First, the effect of varying the thermal sink temperature on the temperature of the thermal radiation source was predicted, using elementary laws of radiative heat transfer. Second, an experiment utilizing a simulated version of the RF-tube test setup was conducted to verify the predicted results. The following conditions were considered in the predictions:

Case 1. Minimum and maximum tube operating power while in a free-space environment.

Case 2. Minimum and maximum tube operating power while in a vacuum chamber exposed to a heat sink at 373°K (boiling water temperature), 300°K (room temperature), and 77°K (LN_2 temperature).

To obtain a model of the tube and a temperature control model for the heat transfer mechanism, the following assumptions were made:

(1) Surface characteristics as given in Fig. 7 and Table 2.

(2) Heat transfer mechanism:

(a) All the radiant energy that leaves the source reaches the plate, even if it must be reflected by the walls.

(b) The radiant energy which is emitted and reflected by the plate is diffusive and a shape area factor must be used in computing the quantity of radiation emitted by the temperature control plate and received by the tube. The radiation reflected and emitted by the walls is neglected.

As a model for this heat transfer mechanism, consider the radiant heat transfer between two parallel disks, Fig 8.

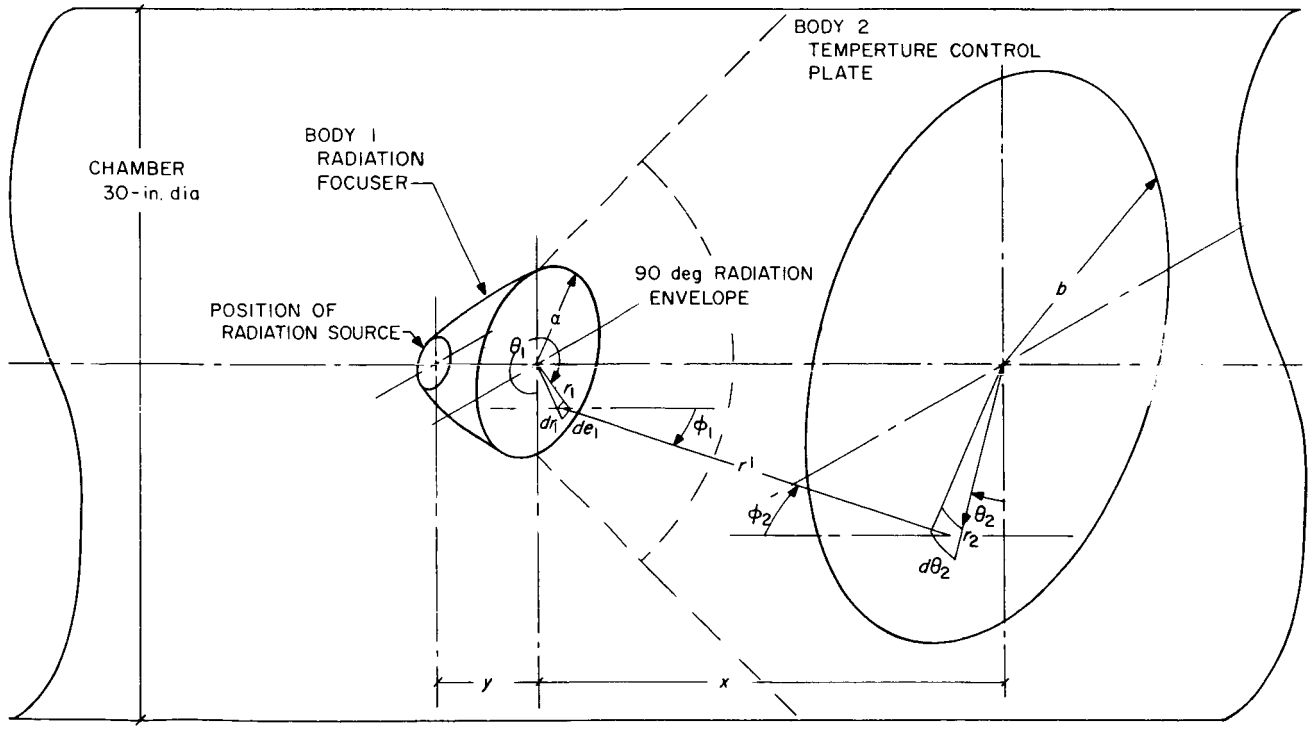

Fig. 8. Heat transfer model

The large disk, body 2, is held at a uniform temperature T_2. The small disk, body 1, approximates the tube radiation source and focusing apparatus. T_1 is the temperature of the tube's radiation source.

1. Case 1

Determination of operating temperature T_1 for two sizes of tubes operating at maximum and minimum power looking at free space at 4°K.

Power radiated = area × emissivity × Stefan-Boltzmann constant $(T_1^4 - 256°K^4)$

(1) For 100–500 w tubes: Area = 4.15 in.^{2}; $\epsilon = 0.9$;

$$\sigma = 36.8 \times 10^{-12} \frac{\text{w}}{\text{in.}^2(°\text{K})^4}$$

(1a) $500\,\text{w} = 4.15\,\text{in.}^2 \times 0.9 \times 36.8 \times 10^{-12} \times T_1^4$

$$T_1 = 1380°\text{K}$$

(1b) $100\,\text{w} = 4.15\,\text{in.}^2 \times 0.9 \times 36.8 \times 10^{-12} \times T_1^4$

$$T_1 = 921°\text{K}$$

(2) For 20–100 w tubes: Area = 0.85 in.^{2}; $\epsilon = 0.9$;

(2a) $100\,\text{w} = 0.85\,\text{in.}^2 \times 0.9 \times 36.8 \times 10^{-12} \times T_1^4$

$$T_1 = 1374°\text{K}$$

(2b) $20\,\text{w} = 0.85 \times 0.9 \times 36.8 \times 10^{-12} \times T_1^4$

$$T_1 = 926°\text{K}$$

2. Case 2 (Fig. 9)

Assuming Lambert's Law for diffusive radiation, the shape area factor for the test setup geometry is:

$$FA = \int_0^{2\pi} \int_0^{b} \int_0^{2\pi} \int_0^{a} \frac{\cos\phi_1 \cos\phi_2 \, r_2 \, dr_2 \, d\theta_2 \, r_1 \, dr_1 \, d\theta_1}{\pi (r^1)^2}$$

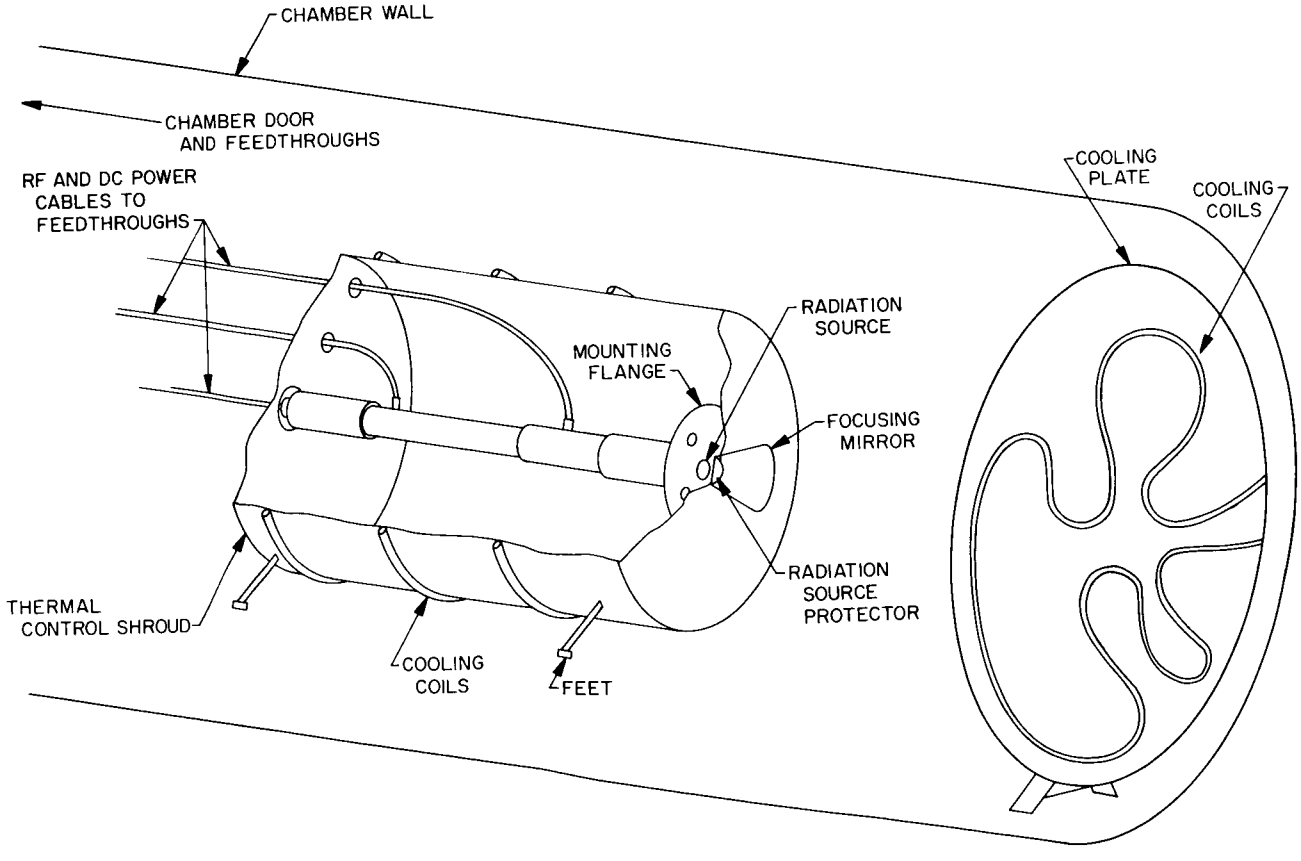

Fig. 9. Conceptual space chamber configuration for traveling wave tube

Where ϕ_1, ϕ_2, and r^1 depend on θ_1, θ_2, r_1, and r_2, and $\phi_1 = \phi_2$. To simplify this expression and obtain an upper bound, let $\phi_1 = \phi_2 = 0$ and $r^1 = x$

$$FA < \frac{2\pi\, 2\pi \times \frac{1}{2} a^2 \frac{1}{2} b^2}{\pi x^2}$$

This expression is evaluated for radii representing likely values of radius a and b, and several values of distance between plate and dish in Table 3.

Table 3. *FA evaluations*

x, in.	Radius, in. (b = 12 in.)		
	a = 4	a = 3	a = 2
		FA, in.^{2}	
8	112.5	63.5	28.4
14	36.8	20.8	9.25
20	18.0	10.2	4.52

It is known that all the tubes under consideration will be approximately 50% efficient. Therefore, if the tube produces X watts of RF power, an equal amount of heat flux from the tube to the surroundings is also produced. The radiation reflected from the surroundings is assumed to come entirely from the plate.

$$Y = FA\left[\rho_2 \frac{Z}{\text{Area Plate}} + \epsilon\, \sigma\, T_2^4\right]$$

$$Y = FA\left[0.1 \frac{Z}{450 \text{ in.}^2} + 0.9 \times 36.8 \times 10^{-12} \times T_2^4\right]$$

$$Y = FA\left[\frac{0.00022Z}{\text{in.}^2} + 33.1 \times 10^{-12} \times T_2^4\right] \quad (1)$$

If all the heating power is radiated, the total radiation by tube Z will equal the quantity X plus the radiation back from surroundings Y, assuming that the radiation back from the surroundings is diffusive, by Lambert's law.

$$\left[1 - FA \frac{(0.00022)}{\text{in.}^2}\right] Z = X + \left[33.1 \times 10^{-12} \frac{w}{\text{in.}^2\,(°K)^4} \times T\right] FA \quad (2)$$

If all this radiation is absorbed by the tube radiation source, in order to obtain an equilibrium condition,

$$T_1 = \left[\frac{Z}{A_1\, \epsilon_1\, \sigma_1}\right]^{1/4} = \left[\frac{(Z \times 10^{12} \text{ in.}^2\, °K^4)}{A_1 \times 33.1 \times w}\right]^{1/4} \quad (3)$$

3. The Experiment

The experiment provided a verification of the results of the analysis. The testing consisted of operating the heat source (simulated heat load of operating traveling wave tube) at three discrete power levels while varying the test shroud temperature in a vacuum environment of less than 1×10^{-4} torr. The temperature of the heat source was lower than predicted for the traveling wave tube because of a different shape area factor.

4. Test Set-up (Fig. 10)

a. Temperature control. The temperature control system consisted of a black drum-like copper shroud with ½-in. copper tubing soldered around its outside surface. LN_2 and GN_2 were circulated through the tubing to control the temperature of the shroud. The shroud and specimen temperatures were monitored using copper-constantan thermocouples and a temperature potentiometer.

b. Heat source. The heat source consisted of a Chromalox heater element installed on a mirror reflector (Fig. 11). The heater was rated 500 w at 120 v.

The heat source was mounted in the chamber with the element placed parallel to and 8 in. from the rear of the chamber (Fig. 12). Two chromel alumel thermocouples were resistance welded to the element, Nos. 6 N and 7 S. These thermocouples were read on the millivolt potentiometer. Power was supplied to the heater on No. 16 copper wire by a variac located outside the chamber and was measured on a wattmeter. One copper constantan thermocouple was bolted to the reflector and was monitored on a temperature potentiometer.

5. Test Program

The chamber was pumped down to less than 10^{-4} torr.

(1) The shroud temperature was adjusted to the required level.

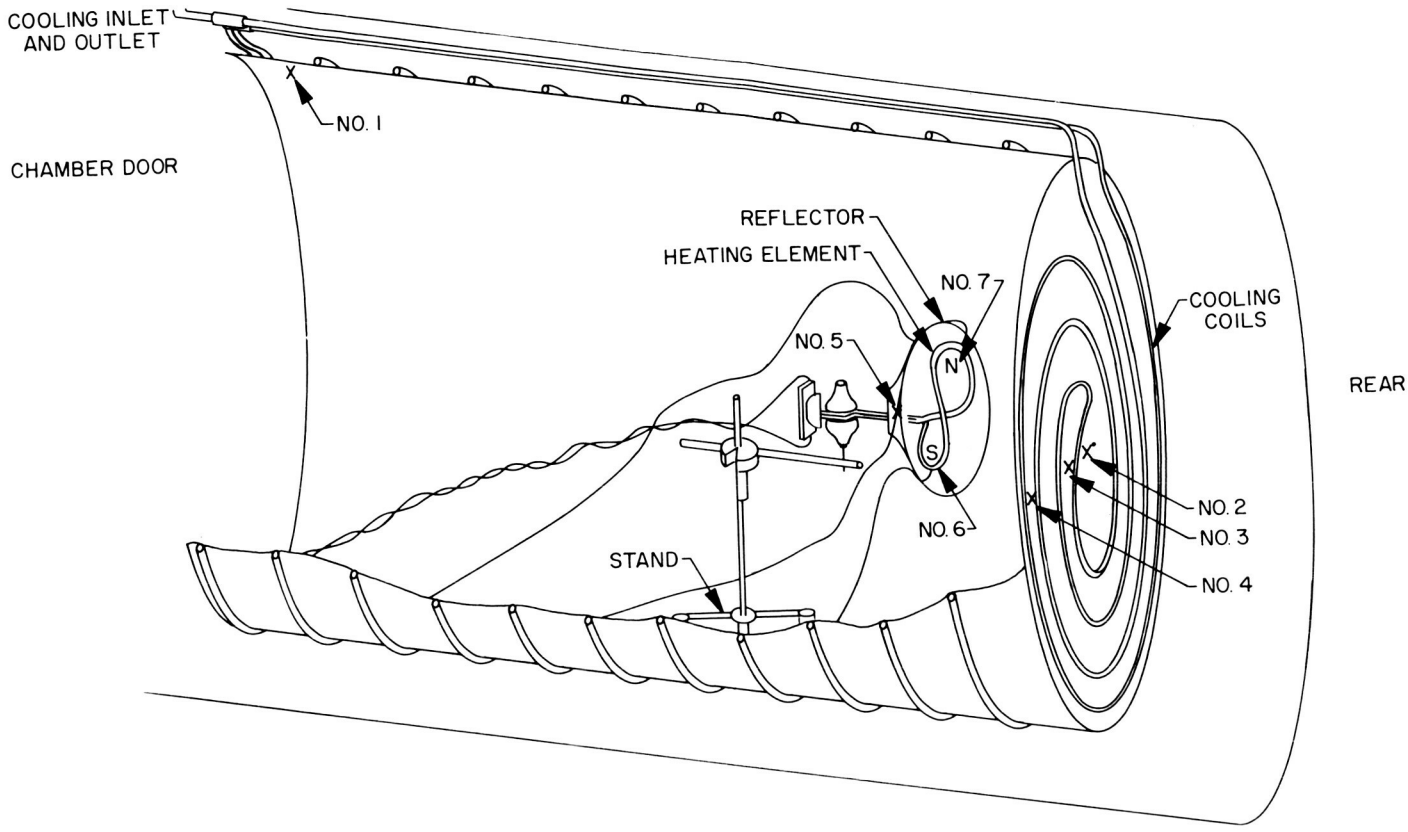

Fig. 10. Setup of experiment

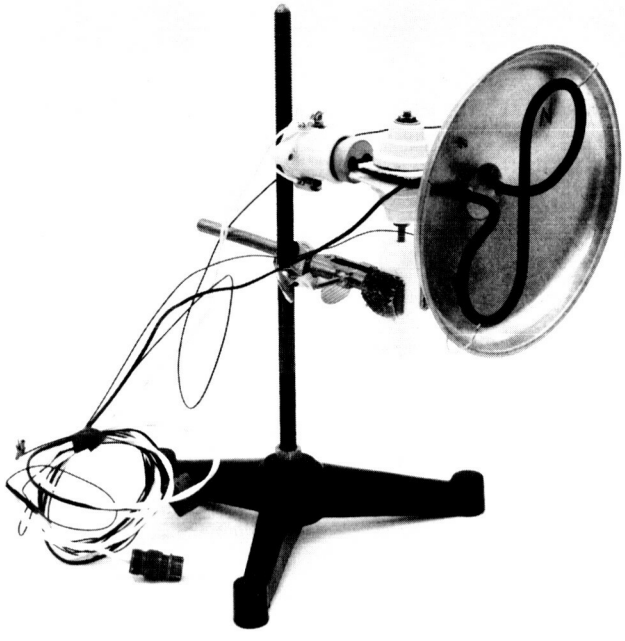

Fig. 11. Heat source used in experiment

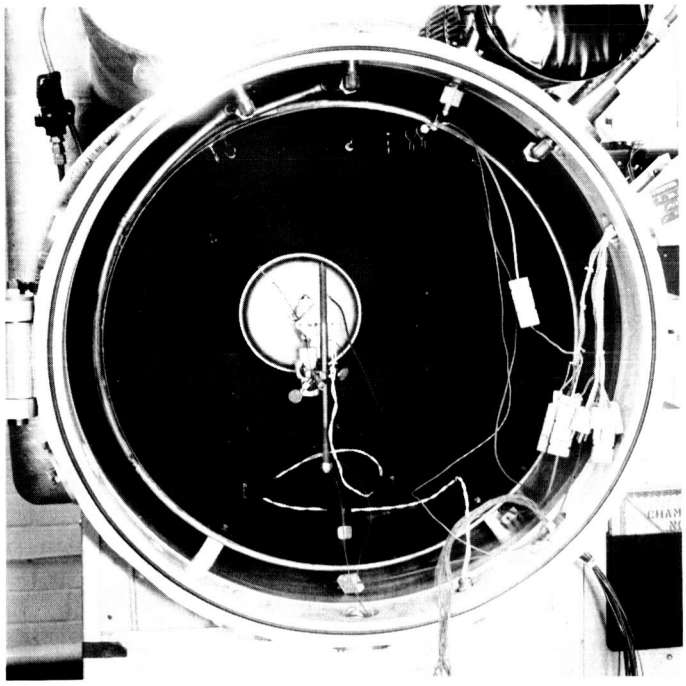

Fig. 12. Heat source shown installed in vacuum chamber

(2) The system was stabilized with the heat source dissipating the selected power, and all the thermocouples were read (Table 4).

Table 4. Comparison of predicted temperature T_1 and experimental temperature data, °K

Element	Temperature °K			
Heat sink	77	300	373	
Small tube at 20 w	926	1118	1218	$T_1 = \left[\frac{Z \times 10^{12}}{A_1 \times 33.1}\right]^{1/4}$ (Case 2)*
Small tube at 100 w	1374	1436	1500	
Large tube at 100 w	921	968	1005	
Large tube at 500 w	1380	1399	1415	
Heat sink temp, °K	88	295	375	
Chromolox Heater at 20 w	523	511	528	T. C. No. 7 (See Fig. 11)
Chromolox Heater at 100 w	749	756	760	
Chromolox Heater at 500 w	1083	1105	1106	

*Assuming $a = 3$ in., $b = 12$ in. and $x = 8$ in.
Note that the shape area factor for the Chromolox Heater was not determined.

(3) Temperature stabilization for this test system was defined as follows:

(a) Heating element: No observable change in temperature over a 3-min period.

(b) Reflector: A change of less than 2°K in 5 min.

(c) Shroud: The temperature of the control thermocouple was cycling about the desired value.

(4) The readings from thermocouples 2–4 showed considerable temperature cycling of the end of the shroud, $\Delta = 4°K$ in the 20-w 88°K-steps and $\Delta = 30°K$ in the 500-w 300°K-steps.

(5) To avoid the control cycling showing as temperature gradients, thermocouples 1–4 were read at the same time.

(6) The modes of temperature control used in this test were:

(a) Only LN_2 cooling for 88°K parts.

(b) Both GN_2 cooling and heating for 300°K part.

(c) Both GN_2 cooling and heating for 366°K part.

6. Conclusions

Two conclusions of primary importance to the transmitter tube development tests are:

(1) The present nitrogen heat exchanger system can maintain any cooling plate temperature in the usual operating range against any power up to 500 w. At no time during the experiment was capacity cooling required.

(2) Varying the shroud temperature had a small effect on the temperature of the heating element. The heat source operated at approximately 500°K, considerably lower than the probable operating temperature of the transmitter tubes. The temperature of the transmitter tube heat radiator would be raised very little by reflection from a test setup similar to that which was used for this experiment.

From a temperature control standpoint, these RF-tube development tests can be easily performed in a 30 × 50 in. vacuum chamber with simple modifications to accommodate the transmitter tubes auxiliary equipment.

References

1. Usher, T., "Simplification of Random Vibration," *Test Engineering*, September 1960.

2. Firestone, F. A., "The Mobility of Computing the Vibration of Linear Mechanical and Acoustical Systems: Mechanical-Electrical Analogies," *Journal of Applied Physics*, Vol. 9, June 1938, pp. 373–387.

3. Cheng, D. K., *Analysis of Linear Systems*, Addison-Wesley Publishing Company, Inc., 1961, p. 58.

References (Cont'd)

4. D'Azzo, J. J. and Houpis, C. H., *Feedback Control System Analysis and Synthesis,* McGraw-Hill Book Co., 1960, p. 94.

5. Hofmeister, L. D., private communication.

6. McCracken, D. D., *A Guide to Fortran IV Programming,* John Wiley & Sons, Inc., 1965, p. 46.